ARTICLES
https://doi.org/10.1038/s41929-020-0423-3

nature catalysis

Check for updates

Enhanced photocatalytic alkane production from fatty acid decarboxylation via inhibition of radical oligomerization

Zhipeng Huang[1,2,3], Zhitong Zhao[1,2,3], Chaofeng Zhang[1], Jianmin Lu[1], Huifang Liu[1], Nengchao Luo[1,2], Jian Zhang[1] and Feng Wang[1]✉

The decarboxylation of bio-derived fatty acids provides a sustainable pathway for the production of alkane products under mild conditions; however, products are generally obtained in low selectivity due to the uncontrollable reactivity of radical intermediates. Here we demonstrate that photogenerated radicals can be rapidly terminated by surface hydrogen species during photocatalytic decarboxylation of fatty acids on a hydrogen-rich surface that is constructed by the interactions between H_2 and Pt/TiO_2 catalyst, thereby greatly inhibiting oligomerization; C_{n-1} alkanes can therefore be obtained from bio-derived C_{12}–C_{18} fatty acids in high yields (≥90%) under mild conditions (30 °C, H_2 pressure ≤0.2 MPa) and 365 nm light-emitting dode irradiation. Industrial low-value fatty acid mixtures (namely, soybean and tall oil fatty acids) can be transformed into alkane products in high yields (up to 95%). Our research introduces an efficient biomass-upgrading approach that is enabled by subtle control of the radical intermediate conversion on a heterogeneous surface.

Long-chain alkanes are among the most important chemicals in modern society as they are the major components in diesel and jet fuel and can be used as feedstocks for olefin and aromatic production[1]. The production of such alkanes from renewable biomass instead of fossil resources is very attractive and important for sustainable energy and chemical supply[2–4]. In this context, bio-derived fatty acids are promising candidates, owing to their inherent structural similarities to diesel-type hydrocarbons, inedible nature, abundance and low cost[5–7]. A substantial amount of fatty acids are produced as low-value by-products in fat and oil processing and the pulp industry[7–9].

Fatty acids can be transformed into alkanes via hydrodeoxygenation; however, most of the established catalytic systems require harsh conditions (reaction temperatures ≥250 °C, H_2 pressures ≥2 MPa) that lead to intensive energy input and excessive H_2 consumption (≥3 molar ratio of H_2 per reactant)[6,10,11]. Alternatively, hydrodecarbonylation and decarboxylation of fatty acids consume less or no H_2, but elevated temperatures (≥300 °C) are required for C–C bond scission and are accompanied by unwanted cracking and coke deposition[10,12–14]. Such harsh reaction conditions dramatically challenge the overall energy efficiency of the proposed alkane synthesis, so a method capable of efficiently converting fatty acids into alkanes under mild conditions (ambient temperature, low reaction pressure) with minimal H_2 consumption is greatly desired.

Oxidative decarboxylation offers a method for fatty acid utilization under much milder conditions (reaction temperatures ≤80 °C, ambient pressure)[15,16], but the production of alkanes is dramatically challenged by the reactivity of radical intermediates; for instance, the alkane mixtures were always obtained in low selectivity (<50%)[17–19] for the photocatalytic decarboxylation of acetic acid and propionic acid over TiO_2-based catalysts in aqueous solution. The generated radicals always tend to form chain-elongated products via C–C radical coupling[20–22]. Walton and colleagues investigated the homocoupling of radicals derived from carboxylic acid decarboxylation over Pt/TiO_2, but the product yields varied markedly with different substrates[21,22], implying the uncontrollable reactivity of radical intermediates. Moreover, the radicals can successively oxidize to the corresponding cations, which subsequently form unwanted ethers, esters and even oligomeric hydrocarbons[23–25]; however, for the conversion of various fatty acids that contain 12 to 22 carbon atoms (which can be obtained from biomass processing in large quantities[1,7]), only alkyl radicals quenched by hydrogen yield the desired diesel-range C_{n-1} alkanes. Wallentin et al.[26] and Nicewicz et al.[27] reported that homogeneous acridinium photocatalysts can achieve the hydrodecarboxylation of various carboxylic acids, but remain inefficient in the production of C_{n-1} alkanes from long-chain fatty acids (yield <50%). Consequently, controlling the conversion of radical intermediates towards preferential termination with hydrogen while inhibiting C–C radical coupling and radical oxidation remains a great challenge.

Herein we report a photocatalytic decarboxylation route for alkane production from bio-derived fatty acids under mild conditions (ambient temperature, $p_{H_2} \leq 0.2$ MPa). Long-chain alkanes can be obtained in ≥90% yield from fatty acids by using a Pt/TiO_2 catalyst under illumination. Interaction between the catalyst and H_2 forms a hydrogen-rich surface that promotes rapid radical termination with surface hydrogen species, thus efficiently inhibiting radical dimerization and oxidation reactions. The consumption of H_2 during this decarboxylation process is negligible owing to its integrated photoredox cycle wherein photogenerated holes convert fatty acids into C_{n-1} alkyl radicals that are subsequently combined with the hydrogen generated through electron-mediated reduction of the carboxyl protons, yielding C_{n-1} alkanes (Fig. 1).

[1]State Key Laboratory of Catalysis, Dalian National Laboratory for Clean Energy, Dalian Institute of Chemical Physics, Chinese Academy of Sciences, Dalian, China. [2]University of Chinese Academy of Sciences, Beijing, China. [3]These authors contributed equally: Zhipeng Huang, Zhitong Zhao. ✉e-mail: wangfeng@dicp.ac.cn

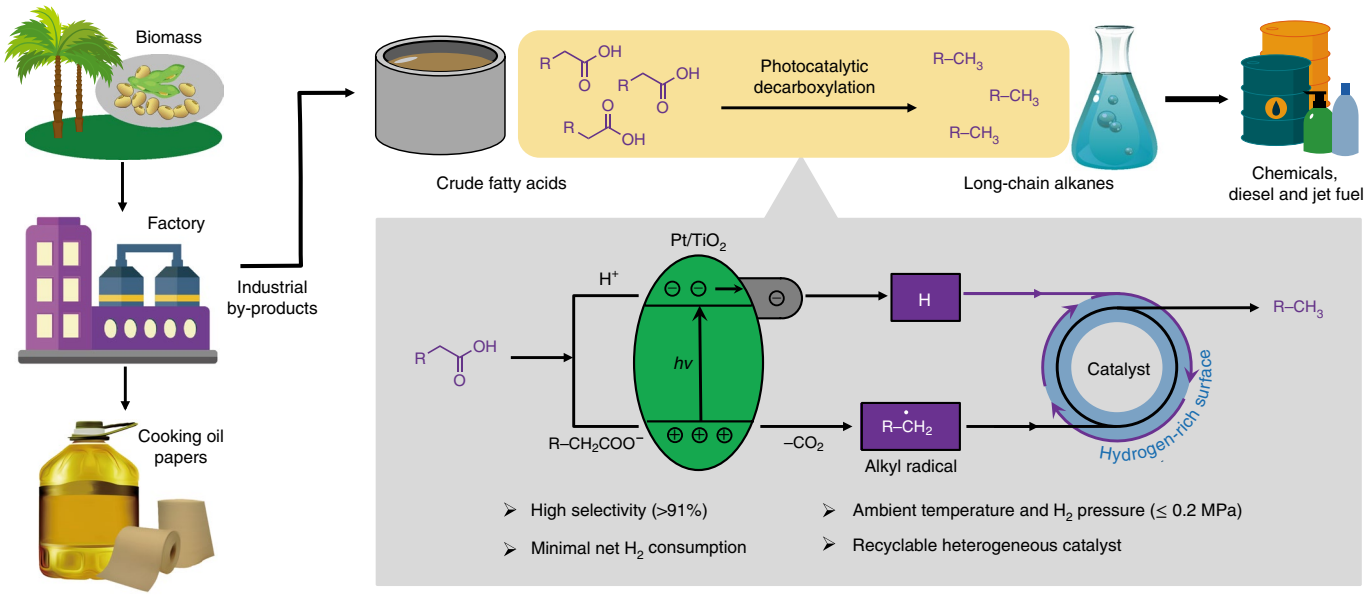

Fig. 1 | A schematic representation of a photocatalytic decarboxylation strategy for the production of alkanes from bio-derived fatty acids. The photocatalytic decarboxylation procedure is highlighted, and the interactions between photogenerated carriers (holes and electrons) and fatty acids are schematically shown in the photoredox cycle.

Results

Photocatalytic decarboxylation of saturated fatty acids. We first performed the photocatalytic conversion of saturated fatty acids in an inert atmosphere. Previous reports reveal that TiO_2 and TiO_2-based catalysts can efficiently degrade carboxylic acids under illumination in spite of poor selectivity for alkane products (<50%)[17–19]; TiO_2 and a series of metal/TiO_2 catalysts were thus screened first, among which Pt/TiO_2 displayed the highest activity for fatty acid conversion after light-emitting diode (LED) irradiation for 80 min (Fig. 2a), yielding *n*-heptadecane as the only detected product in gas chromatography analysis. Other metal oxide semiconductors with platinum deposits showed poor or negligible activity for the conversion of stearic acid, demonstrating the vital role of TiO_2 for the photocatalytic decarboxylation. Consequently, Pt/TiO_2 was chosen for further study. After LED irradiation for 2 h, stearic acid, palmitic acid and lauric acid—which are the most abundant saturated fatty acids in biolipids—were almost completely converted over Pt/TiO_2, but the desired C_{n-1} alkanes were only obtained in a moderate selectivity (60–74%) (Fig. 2b). Control experiments with a radical trapping agent and fatty acid mixture revealed the existence of active C_{n-1} alkyl radical intermediates that were generated from hole-mediated decarboxylation (Supplementary Figs. 1 and 2)[16,28]. Substantial amounts of complex high-carbon hydrocarbons derived from radical dimerization, radical oxidation and successive oligomerization were detected (Fig. 2c and Supplementary Fig. 3)[23,25], accounting for the unsatisfied selectivity of the desired C_{n-1} alkanes. As the C_{n-1} alkanes are derived from the combination of alkyl radicals and hydrogen, further conversion of generated C_{n-1} alkyl radicals over Pt/TiO_2 (oligomerization versus hydrogen quenching) determines the product distribution.

In previous reports, the products derived from photogenerated radicals varied dramatically for different carboxylic acids over TiO_2 (refs. [21,22]), indicating the uncontrollable reactivity of the alkyl radicals on TiO_2 surface. We assumed that (as an alternative approach) boosting the hydrogen available to the alkyl radicals ought to facilitate the rapid quenching by hydrogen, thus restraining the unwanted oligomerization reactions. In view of this, we changed the inert reaction atmosphere to H_2 (0.1 MPa). Surprisingly, the selectivity of the C_{n-1} alkanes increased markedly (≥91%) and a particularly high selectivity of 96% was obtained for stearic acid conversion. As such, the formation of oligomeric hydrocarbons was dramatically suppressed (Fig. 2b,c). In comparison with other metal/TiO_2 catalysts, Pt/TiO_2 still displayed the highest conversion and selectivity for *n*-heptadecane production from stearic acid (Supplementary Fig. 4; more optimizations of the reaction conditions are listed in Supplementary Table 1). Acetonitrile was deemed to be the most suitable solvent, and decreasing the catalyst concentration and metal loading both led to lower conversion and C_{n-1} alkane yield. Control experiments without catalyst or LED irradiation offered no conversion of fatty acid, indicating that this is a photocatalytic process.

Influence of H_2 on the production of C_{n-1} alkanes. Compared with an inert atmosphere, H_2 did not alter the conversion rates of fatty acids over Pt/TiO_2 (Supplementary Fig. 5), but consderably promoted the production of the desired C_{n-1} alkanes, demonstrating that the interaction between H_2 and the Pt/TiO_2 catalyst plays an important role in the preferential combination of alkyl radicals and hydrogen. The Pt/TiO_2 catalyst was synthesized by an impregnation–calcination method, its powder X-ray diffraction (XRD) spectra reveal a characteristic pattern of mixed-phase TiO_2 (Degussa P25) and no diffraction pattern of platinum was observed (Supplementary Fig. 6). The transmission electron microscopy (TEM) image shows that platinum nanoparticles are uniformly dispersed on TiO_2 surface with a small average size of 1.7 ± 0.4 nm (Fig. 3a). In the X-ray photoelectron spectra of Pt/TiO_2, the binding energy of Pt $4f_{7/2}$ (71.3 eV) corresponds to metallic platinum on TiO_2 (Supplementary Fig. 6)[29], which is consistent with the result of CO-absorption Fourier transform–infrared (FT-IR) spectra. The bands at around 2,060 cm^{-1} and 1,821 cm^{-1} can be assigned to vibrations of linearly adsorbed and multibonded CO on metallic platinum, respectively[30,31]. These results illustrate that platinum nanoparticles are highly dispersed on TiO_2 in metallic form; hence, H_2 can activate and dissociate on platinum nanoparticles at ambient temperature[32]. Moreover, platinum can efficiently accumulate photogenerated electrons for the reduction of the protons derived from fatty acid dissociative adsorption (Supplementary Figs. 7 and 8)[33,34]; hydrogen dissociation and proton reduction therefore together enrich hydrogen on the platinum nanoparticles when the reaction proceeds in a H_2 atmosphere.

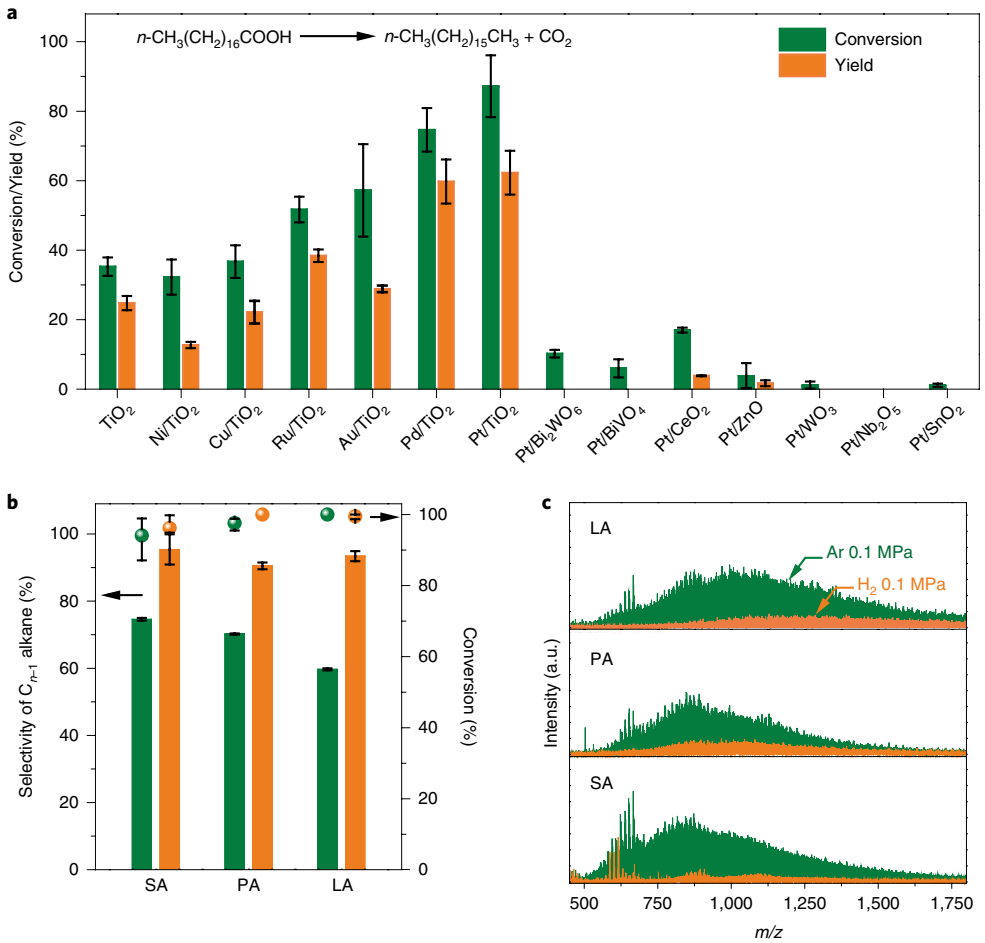

Fig. 2 | Photocatalytic decarboxylation of saturated fatty acids. a, Photocatalytic decarboxylation of stearic acids over different catalysts in argon (0.1 MPa) atmosphere with LED irradiation for 80 min. **b**, Photocatalytic decarboxylation of saturated fatty acids in argon (0.1 MPa, green) and H_2 (0.1 MPa, orange) atmosphere over Pt/TiO_2, where the bars indicate the selectivity of C_{n-1} alkane percentage and the scatter dots indicate the conversion percentage. SA, stearic acid; PA, palmitic acid; LA, lauric acid. **c**, Matrix-assisted laser desorption/ionization-time of flight mass spectrometer (MALDI-TOF MS) patterns after the conversion of different saturated fatty acids over Pt/TiO_2 in argon and H_2 atmosphere. Reaction conditions: catalyst (10 mg), fatty acid (0.05 mmol), acetonitrile (1.50 ml), reaction pressure (0.1 MPa), LED (365 nm, 18 W) irradiation for 120 min, 30 °C. Conversion and selectivity were determined by gas chromatography analysis. The error bars represent the relative deviation derived from parallel experiments.

Table 1 | The results of industrial crude fatty acids conversion over Pt/TiO_2[a]

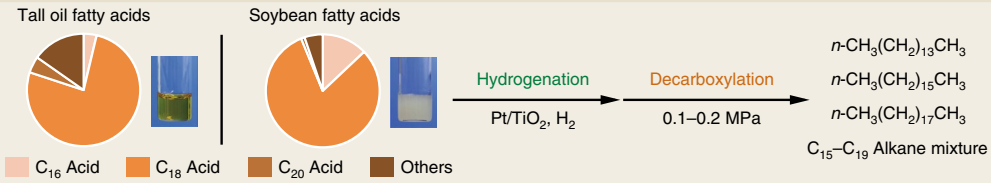

Entry	Feedstock	H_2 pressure (MPa)	Conversion (%)	Molar yield of C_{n-1} alkane (%)					CO_2 yield (%)[b]	Carbon balance (%)[c]
				n-C_{15}	*n*-C_{17}	*n*-C_{19}	Others	Total		
1	TOFA	0.1	98	5	70	3	1	79	59	80
2	SBFA	0.1	97	13	73	<1	<1	87	59	88
3	TOFA	0.2	98	4	74	4	2	83	74	85
4	SBFA	0.2	93	15	76	<1	<1	92	66	97
5[d]	SBFA	0.2	97	15	79	1	<1	95	68	96

[a]Reaction conditions: industrial crude fatty acids (15 mg), catalyst Pt/TiO_2 (10 mg), acetonitrile (1.50 ml), H_2 atmosphere, the reaction solvent was stirred at ambient temperature in a H_2 atmosphere in the dark for 60 min, followed by LED irradiation (365 nm, 18 W) for 120 min at 30 °C. [b]Carbon dioxide adsorption on the catalyst and dissolution in the solvent result in moderate yield. [c]The formation of oligomeric hydrocarbons mainly accounts for the carbon loss. [d]Extra water (12 wt% with respect to feedstock) was added.

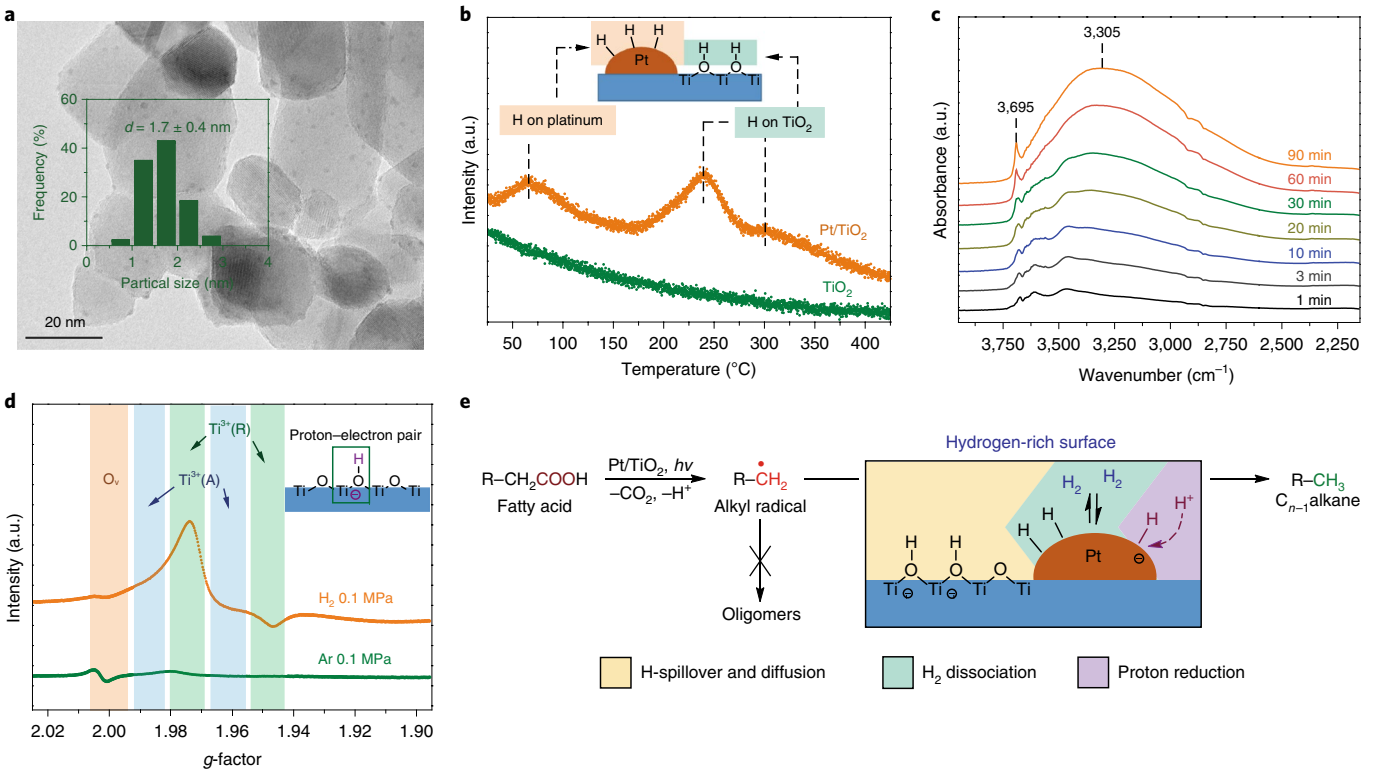

Fig. 3 | The interaction between H_2 and Pt/TiO_2 and its influence on the production of C_{n-1} alkanes. a, A TEM image of the Pt/TiO_2 catalyst and a size distribution (where *d* is diameter) of the platinum nanoparticles on Pt/TiO_2. **b**, H_2-TPD profiles of Pt/TiO_2 and TiO_2 after exposure to H_2 at ambient temperature. **c**, A FT-IR spectra of Pt/TiO_2 in H_2 atmosphere for different exposure times. **d**, An EPR spectra of Pt/TiO_2 in different atmospheres. O_v, Ti^{3+}(R) and Ti^{3+}(A) represent the EPR signals of oxygen vacancies, Ti^{3+} on rutile TiO_2 and Ti^{3+} on anatase TiO_2, respectively. **e**, Plausible reaction pathways for the photocatalytic decarboxylation of fatty acids over Pt/TiO_2 in a H_2 atmosphere.

However, given the fact that the alkyl radicals are generated by holes on TiO_2 (Supplementary Fig. 8), there is a spatial separation between the hydrogen on the isolated platinum nanoparticles and the alkyl radicals on the broad TiO_2 surface. Hydrogen enrichment on the platinum nanoparticles therefore does not directly account for the preferential radical quenching with hydrogen. Hydrogen-temperature-programmed desorption (H_2-TPD), in situ FT-IR and electron paramagnetic resonance (EPR) studies were carried out to obtain further insight into this process. After exposure to H_2 atmosphere at room temperature, the hydrogen species formed on Pt/TiO_2 could be revealed by a H_2-TPD study (Fig. 3b). The low-temperature peak can be assigned to desorption of hydrogen on metallic platinum, whereas the desorption peaks above 200 °C are relative to hydrogen species on TiO_2 derived from hydrogen spillover[30]. Moreover, the interaction between H_2 and Pt/TiO_2 forms hydroxyls on TiO_2, as seen in the in situ FT-IR spectra (Fig. 3c). When Pt/TiO_2 was exposed to a H_2 atmosphere, an absorption band near 3,700 cm^{-1} immediately appeared and grew in intensity with prolonged exposure time, which can be assigned to O–H stretching modes of isolated surface hydroxyls[35]. Meanwhile, a broad band located near 3,370 cm^{-1} gradually developed and shifted to 3,305 cm^{-1} as the exposure time prolonged, demonstrating the formation of self-associated surface hydroxyls with interspecies hydrogen bonding as a result of continuous hydroxyl development[36]. These results evidently verify the occurrence of hydrogen spillover from platinum onto TiO_2. Furthermore, exposure to H_2 led to the partial reduction of TiO_2 on Pt/TiO_2, as revealed by EPR spectra (Fig. 3d). In an inert atmosphere, there are only some weak signals of oxygen defects that were formed during the preparation process[37]. By contrast, when Pt/TiO_2 was exposed to H_2 atmosphere, strong signals for Ti(III) centres on both anatase and rutile phase of TiO_2 were observed[38], indicating the proton–electron pair nature of hydrogen on TiO_2 (ref. [39]). Along with the proton of the hydroxyl, an electron is localized on the adjacent Ti(IV) site, which leads to the partial reduction of TiO_2 (Fig. 3d); thus, in addition to the active hydrogen on the platinum nanoparticles, the neutral proton–electron pair on TiO_2 can also participate in alkyl radical quenching to yield alkane products via a heterogeneous proton-coupled electron transfer process[40]. Consequently, along with proton reduction and H_2 dissociation, hydrogen spillover from platinum onto TiO_2 forms a hydrogen-rich surface with abundant hydrogen on both platinum and TiO_2, which facilitates rapid alkyl radical quenching with hydrogen before oligomerization (Fig. 3e) and results in high selectivity of the desired alkane. The highly dispersed metallic platinum nanoparticles and fast migration of hydrogen on TiO_2 substantially contribute to the development of such a hydrogen-rich surface (Fig. 3a and Supplementary Fig. 9)[41].

Furthermore, the hydrogenation of CO_2—a hydrogen-consuming side-reaction that usually occurs at high temperatures[42]—did not occur in our system because of the moderate reaction conditions (ambient temperature, low H_2 pressure, Supplementary Fig. 5). Although H_2 was employed to form a hydrogen-rich atmosphere, the net H_2 consumption was minimal in our integrated photoredox cycle as the photogenerated electrons reduce protons to compensate for the continuous consumption of the surface hydrogen by the hole-induced alkyl radicals. In an inert atmosphere, H_2 evolution reduced the surface hydrogen on the catalyst (Supplementary Fig. 5), the alkane products were obtained only in moderate selectivity as a result. A specific H_2 partial pressure (≥0.1 MPa) was required not only to compensate for the hydrogen loss due to H_2 evolution, but also to steer the hydrogen flow to boost the surface hydrogen concentration (Supplementary Fig. 10) as hydrogen

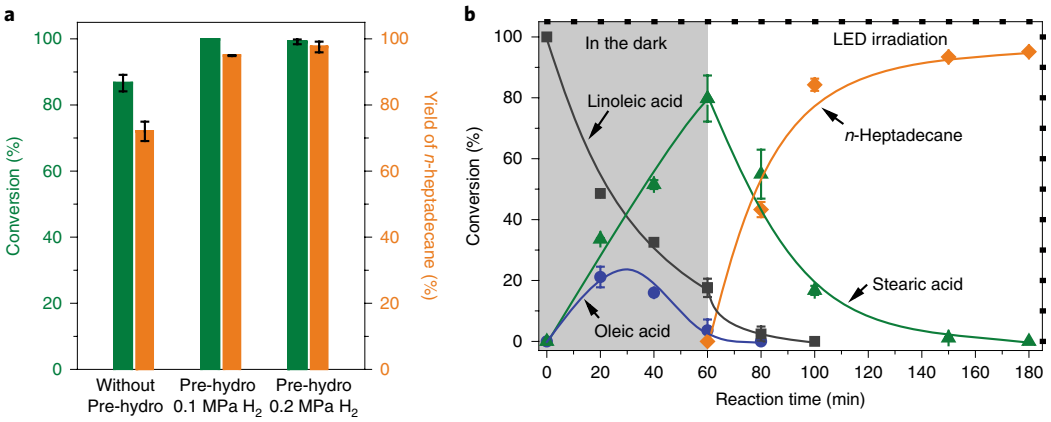

c

Entry	Feedstock	Product	Conv. (%)	Yield (%)
1	Stearic acid	*n*-Heptadecane	96 95[a]	92 80[a]
2	Oleic acid	*n*-Heptadecane	98	90
3[b]	Linoleic acid	*n*-Heptadecane	>99	95
4	Palmitic acid	*n*-Pentadecane	>99	91
5[c]	Lauric acid	*n*-Hendecane	>99	93
6[b]	Linoleic acid and palmatic acid (mol ratio = 1:1)	*n*-Heptadecane *n*-Pentadecane	99	93
7[c]	Palmitic acid and lauric acid (mol ratio = 1:2)	*n*-Pentadecane *n*-Hendecane	>99	94

Fig. 4 | Photocatalytic decarboxylation of unsaturated fatty acids and fatty acid mixtures over Pt/TiO_2. a, The influence of pre-hydrogenation (pre-hydro) on the photocatalytic decarboxylation of linoleic acid over Pt/TiO_2 under LED (365 nm, 18 W) irradiation for 120 min. Pre-hydrogenation means that the reaction solvent was stirred at ambient temperature in a H_2 atmosphere in the dark for 60 min before LED irradiation. **b**, The percentage of fatty acids and alkane products as a function of time in the hydrogenation–photocatalytic decarboxylation of linoleic acid over Pt/TiO_2 in a H_2 atmosphere (0.1 MPa). **c**, Photocatalytic decarboxylation of various bio-derived fatty acids and their mixtures over Pt/TiO_2 in a H_2 atmosphere (0.1 MPa) under LED (365 nm, 18 W) irradiation for 120 min. [a]Scale-up reaction results for stearic acid (1.0 mmol) conversion under xenon lamp irradiation (300 W). [b]A pre-hydrogenation procedure was employed. [c]Fatty acid(s) (0.075 mmol). The error bars represent the relative deviation derived from parallel experiments. The curves drawn on top of the data are guides to the eye.

spillover is considerably dependent on H_2 pressure[43]. Furthermore, as hydrogen extraction from the solvent by alkyl radicals was ruled out by the isotope-labelled experiments (Supplementary Fig. 11), surface hydrogen species serve as a green and efficient hydrogen source for alkane production in our system, instead of extra organic hydrogen donors[26,27].

After thoroughly investigating the promotion effect of H_2 in the photocatalytic decarboxylation over Pt/TiO_2, we infer that such a rapid radical termination strategy can be applied to other catalytic systems. When using Pd/TiO_2 as a catalyst in the conversion of stearic acid in an argon atmosphere, *n*-heptadecane was obtained with moderate selectivity (77%; Supplementary Fig. 12); however, when changing the inert atmosphere into H_2 (0.1 MPa), the selectivity markedly increased to 92%, which was comparable to that over Pt/TiO_2. It can be further improved to 94% with higher H_2 pressure (0.2 MPa). Detailed characterization revealed that metallic palladium nanoparticles are highly dispersed on TiO_2 (ref. [44]) and a H_2-TPD study verified the occurrence of H_2 dissociation and subsequently hydrogen spillover over Pd/TiO_2 after exposure to H_2 (Supplementary Fig. 12)[45]. Consequently, similar to Pt/TiO_2, a hydrogen-rich surface forms over Pd/TiO_2 in a H_2 atmosphere, thus facilitating the rapid radical termination with surface hydrogen to produce C_{n-1} alkane.

Photocatalytic decarboxylation of unsaturated fatty acids and fatty acid mixtures. Unsaturated fatty acids are the major components of crude fatty acids, thus their conversions over Pt/TiO_2 were also studied by employing linoleic acid as a typical substrate. The hole-induced alkyl radicals tend to attack the unsaturated C=C bonds of the substrate and induce polymerization[46], which impedes the production of desired hydrocarbons. Indeed, *n*-heptadecane was obtained in a moderate yield (71%) over Pt/TiO_2 in a H_2 atmosphere (0.1 MPa) (Fig. 4a), which is markedly lower than that of the saturated stearic acid conversion; however, no alkene was detected, implying the outstanding hydrogenation activity of Pt/TiO_2 under moderate conditions (ambient temperature, low H_2 pressure)[47]. A pre-hydrogenation procedure wherein the reaction solvent was stirred for 60 min at ambient temperatures in a H_2 atmosphere before illumination was carried out to minimize the influence of C=C bonds in the substrate. Such pre-hydrogenation treatment can increase the yield of *n*-heptadecane to 95%, because 80% of the unsaturated fatty acids were converted into saturated ones after

the pre-hydrogenation procedure (Fig. 4b). The yield was further improved to 98% by increasing the H_2 pressure to 0.2 MPa (Fig. 4a). Consequently, unsaturated fatty acids can be efficiently transformed into alkane products via a tandem hydrogenation–photocatalytic decarboxylation procedure over bifunctional Pt/TiO_2.

The reaction results of various bio-derived fatty acids are summarized in Fig. 4c. All of the studied feedstocks can be converted into corresponding C_{n-1} alkanes in high yields (≥90%) at ambient temperature in a H_2 atmosphere (0.1 MPa) (Fig. 4c, entries 1–5). More importantly, when utilizing mixtures of fatty acids as feedstock, different fatty acids can be simultaneously converted, offering alkane products in high yields (Fig. 4c, entries 6 and 7, Supplementary Fig. 13), which implies the potential of our method for industrial crude fatty acids upgrading. In a scale-up reaction of stearic acid, *n*-heptadecane was obtained in a promising yield (80%) over Pt/TiO_2 under simulated solar light irradiation (Fig. 4c, entry 1). It is noteworthy that the average production rates ranged from 2.25 to 3.49 mmol $g_{cat}^{-1} h^{-1}$ for the conversion of different fatty acids in our system; these rates are highly comparable to or even higher than those of the thermocatalytic systems operated under harsh reaction conditions (Supplementary Table 2).

Conversion of industrial crude fatty acids. Encouraged by the above results, the conversion of industrial crude fatty acids was carried out to verify the feasibility of photocatalytic alkane production. Utilizing non-food feedstock for green alkane production is preferred as it avoids competition with the food industry[48,49]. Inedible soybean fatty acids (SBFAs) and tall oil fatty acids (TOFAs), the by-products of soybean oil refinery and the pulp industry, respectively, were thus employed in our research. These fatty acid mixtures are ideal feedstocks because of their low cost, abundance and easy availability[1,7,8]. They mainly consist of saturated and unsaturated C_{16}, C_{18} and C_{20} acids (Supplementary Fig. 14 and Supplementary Table 3); TOFA also comprises ~12 wt% of rosin acids and their derivatives. In a H_2 atmosphere (0.1 MPa), TOFA and SBFA were converted into alkane mixtures in yields of 79% and 87%, respectively (Table 1, entries 1 and 2) through a tandem hydrogenation–photocatalytic decarboxylation procedure; the major products were *n*-pentadecane, *n*-heptadecane and *n*-nonadecane (Supplementary Fig. 15). Increasing the H_2 pressure (0.2 MPa) can suppress side-reactions (Supplementary Fig. 16) and increase the total yield of the desired alkanes to 83% and 92% for TOFA and SBFA conversion, respectively (Table 1, entries 3 and 4). There is a considerable amount of moisture remaining in crude fatty acids depending on the industrial processing and their conversion thus requires a robust water-tolerant catalyst. In our system, the presence of water (12 wt%) in the SBFA had marginal influence on the catalytic activity of Pt/TiO_2 (Table 1, entry 5). Moreover, the Pt/TiO_2 catalyst can be reused for at least four runs without subsantial loss in activity (Supplementary Figs. 17 and 18).

An industrial-scale process flow has been designed and simulated—employing SBFAs as feedstocks—to evaluate the practical potential of our method for green alkane production; the model contains feedstock pre-treatment, photocatalytic reaction and purification units (Supplementary Fig. 19). A steady-state simulation using Aspen plus was conducted to obtain a rigorous material and energy balance based on the current reaction conditions and inventory (Supplementary Fig. 20, Supplementary Tables 4–8). Life-cycle assessment was subsequently performed (Supplementary Fig. 21) and the results reveal that our system is currently uncompetitive in fossil energy saving and climate change mitigation compared with fossil-based diesel production (Supplementary Figs. 22 and 23) due to the high energy consumption. For instance, life-cycle greenhouse gas emissions are 2.7–4.8 fold higher than those of conventional diesel. Here, electricity contributes 60.4–74.9%, depending on regional energy supplies. More efficient electricity utilization is therefore the priority to make our system competitive, which can be achieved through an improved photocatalytic system with higher LED radiant efficiency and a robust photocatalyst with higher apparent quantum efficiency (AQE). Alternative low-carbon electricity supply can also directly make our process greener. Besides, denser substrate flow can reduce the energy for product purification and solvent recovery. Our system could become a green and competitive process with considerable potential in energy conservation and greenhouse gas emission reduction through these synergistic process optimizations (Supplementary Figs. 24–27). At last, a theoretical plant with an annual capacity of 80 kilometric tonnes (kt) of long-chain alkanes was simulated, and it will save about 2 TJ energy and reduce 14.8 kt greenhouse gas emissions with an AQE of 0.15 and a solvent-to-substrate ratio of 20 in a scenario where energy is obtained through photovoltaics.

Conclusion

We have developed a photocatalytic decarboxylation route to efficiently upgrade bio-derived fatty acids into long-chain alkanes under mild conditions (ambient temperature, $p_{H_2} \leq 0.2$ MPa), employing Pt/TiO_2 as a robust and recyclable catalyst. Detailed characterization reveals that in a H_2 atmosphere, a hydrogen-rich surface is formed on Pt/TiO_2, which enhances the rapid combination of photogenerated alkyl radicals and surface hydrogen to yield the desired alkanes in high selectivity. The integrated photoredox cycle leads to a decarboxylation process with negligible H_2 consumption. Various bio-derived fatty acids can be converted into C_{n-1} alkanes in high yields (≥90%) and the average production rates are significantly comparable to those of the thermocatalytic systems operated under harsh reaction conditions (high temperature and reaction pressure). Industrial by-products such as TOFAs and SBFAs can be readily transformed into alkane products in high yields (up to 95%) through a tandem hydrogenation-decarboxylation procedure. Our research represents an efficient approach for biomass upgrading via rational modulation of active intermediate conversion on a heterogeneous surface.

Methods

Materials and reagents. All chemicals are of analytical grade and used as purchased without further purification. Stearic acid (99%) was purchased from Macklin Reagent. Lauric acid (99.5%) was purchased from Energy Reagent. Linoleic acid (>97%), oleic acid (99%), palmitic acid (99%), *n*-heptadecane (99.5%), *n*-pentadecane (99.5%), *n*-hendecane (99.5%) and *n*-dodecane (99%) were purchased from Aladdin Reagent. Soybean fatty acids were purchased from Zibo Fengsen Lipid Chemical. TOFAs (F3) were purchased from Maya Reagent and reaction solvents were purchased from Sinopharm Chemical Reagent. Noble metal salts were purchased from the Non Ferrous Metal Institute of Shenyang.

Catalyst preparation. The Pt/TiO_2 catalyst was prepared by an impregnation–calcination method. TiO_2 (0.5 g, Degussa P25) was added into a 20 ml aqueous solution of H_2PtCl_6 containing 5 mg of platinum. The slurry was stirred at room temperature for 12 h. The solvent was subsequently evaporated at 105 °C and the obtained solid was kept in an oven at 100 °C for 4 h for further dehydration. The dried powder was first calcined in air flow (30 ml min^{-1}) at 400 °C for 4 h. When cooled to room temperature, the calcined sample was further reduced in H_2 flow (30 ml min^{-1}) at 350 °C for 4 h. The heating rate of both procedures was 10 °C per min. Other metal/TiO_2 catalysts (including Ni/TiO_2, Cu/TiO_2, Au/TiO_2, Ru/TiO_2 and Pd/TiO_2) were prepared via a similar method except utilizing $NiCl_2{\cdot}6H_2O$, $CuCl_2{\cdot}6H_2O$, $HAuCl_4$, $RuCl_3{\cdot}xH_2O$ and $PdCl_2{\cdot}xH_2O$ as metal precursors, respectively. Other platinum/metal oxide catalysts (including Pt/CeO_2, Pt/$BiVO_4$, Pt/Bi_2WO_6, Pt/ZnO, Pt/WO_3, Pt/Nb_2O_5, Pt/SnO_2) were prepared via a similar method except utilizing CeO_2, $BiVO_4$, Bi_2WO_6 and commercial ZnO, WO_3, Nb_2O_5, SnO_2 as supports, respectively. CeO_2, $BiVO_4$ and Bi_2WO_6 were prepared according to the literature[50–52]. The content of metal deposition in all mentioned catalysts was 1 wt% relative to oxide supports unless stated otherwise.

Catalytic experiments. Photocatalytic decarboxylation of fatty acids was mainly carried out in a homemade LED photoreactor[4]. Stearic acid (0.05 mmol) and Pt/TiO_2 catalyst (10 mg) were added to 1.5 ml of acetonitrile in a quartz tube with a magnetic bar. The inner atmosphere was repeatedly evacuated by a water pump and recharged with argon (0.1 MPa) five times. The inner atmosphere was then repeatedly evacuated and recharged with H_2 (0.1 MPa) five times. The quartz tube

was then irradiated by an LED (18 W, 365 nm) with continuous stirring at ambient temperature (30 ± 5 °C). The stirring rate was 550–600 rpm. For the conversion of some unsaturated substrates, including linoleic acid and industrial crude fatty acids, the reaction mixture was stirred for 60 min at room temperature before LED irradiation.

Several parallel reactions were carried out in each run of the cyclic test of the catalyst. After the reaction, one of them was chosen for derivatization and then gas chromatography analysis, whereas the catalyst in the rest reactions was separated by centrifugation and washed with hexane and ethanol several times; the catalyst was dried in vacuum at 40 °C for 6 h and then directly used for the next run.

In the scale-up reaction, 1 mmol of stearic acid and 200 mg of Pt/TiO_2 catalyst were added to 30 ml of acetonitrile in a 100 ml Schlenk flask equipped with condenser coil. The inner atmosphere was repeatedly evacuated by a water pump and recharged with argon (0.1 MPa) five times; the inner atmosphere was further evacuated and recharged with H_2 (0.1 MPa) five times. The reaction solvent was subsequently continuously stirred (600 r.p.m) under slow H_2 flow for 3 h to completely remove O_2. A xenon lamp (300 W) fitted with a filter of 250–400 nm was switched on and irradiated for 11 h with continuous water cooling. After the reaction, 30 ml of 1,2-dichloroethane was added and the flask was heated in an oil bath of 70 °C to form a uniform slurry; the volume of slurry was measured by a graduated cylinder. Finally, 3 ml of slurry was utilized for quantitative analysis after derivatization. A slightly lower yield for the scale-up reaction may result from incomplete oxygen replacement in the flask[53].

Product analysis. After the photocatalytic reaction, dodecane (as the internal standard, dissolved in 1,2-dichloroethane solution), 100 µl of N,O-bis(trimethylsiyl)trifluoroacetamide and trimethylchlorosilane mixture (99:1), and 200 µl of pyridine were added in the reaction mixture. The mixture was heated in oil bath (60 °C) for 60 min for derivatization[54]. After filtration with a 0.22 µm Nylon syringe filter, the filtrate was used for further analysis.

The products in the liquid phase were identified by gas chromatography–mass spectrometry (GC-MS, Agilent 7890A/5975C) with a HP-5 column. The injection temperature was 260 °C and the detection temperature was 280 °C. The column temperature was first held at 100 °C for 2 min and increased to 280 °C at a ramp rate of 10 °C per min. Highly pure helium was used as the carrier gas. The liquid products were quantitatively analysed by gas chromatography with a flame ionization detector (Agilent 7890 A) using a HP-5 capillary column. The injection temperature was 260 °C and the detection temperature was 280 °C. The column temperature was first held at 100 °C for 2 min and increased to 280 °C at a ramp rate of 10 °C per min; highly pure N_2 was used as the carrier gas.

MALDI-TOF mass spectrometry (MALDI-TOF/TOF 5800, AB SCIEX) was employed to analyse the oligomeric hydrocarbons. After the reaction, the reaction mixture was mixed with 1.5 ml of toluene by ultrasonic treatment for 5 min. The solid catalyst was subsequently separated by a 0.22 µm Nylon syringe filter and the organic filtrate was used for MALDI-TOF mass spectrometry analysis.

The products in gas phase (CO_2 and H_2) were quantitatively analysed by a mass spectrometer (GSD320 Thermostar) and reaction gas analysis was conducted by Techcomp GC 7900 gas chromatograph (thermal conductivity detector, TDX-01 column).

All of the quantitative experiments were repeated at least twice to guarantee the accuracy of data.

The conversion, yield and selectivity were calculated as mole percent as follows:

$$\text{Conversion (mol\%)} = \left(1 - \frac{n(\text{Feedstock after reaction})}{n(\text{Feedstock before reaction})}\right) \times 100\% \quad (1)$$

$$\text{Yield (mol\%)} = \frac{\sum n(\text{Product})}{n(\text{Feedstock before reaction})} \times 100\% \quad (2)$$

$$\text{Selectivity (\%)} = \frac{\text{Yield (mol\%)}}{\text{Conversion (mol\%)}} \times 100\% \quad (3)$$

For the conversion of industrial crude fatty acids, the alkane yield was calculated as mole percent as follows:

$$\text{Yield (mol\%)} = \frac{\sum n(\text{Product})}{\sum n(\text{Theoretical product})} \times 100\% \quad (4)$$

The carbon balance was calculated as mole percent as follows:

$$\text{Carbon balance(\%)} = \frac{\sum n(\text{Product}) + n(\text{Feedstock after reaction})}{n(\text{Feedstock before reaction})} \times 100\% \quad (5)$$

The hydrocarbon oligomers formed by the alkyl radicals have a continuous and wide molecular weight distribution ranging from 400 to 1,800 according to the MALDI-TOF mass spectrometry analysis and so they can not be accurately quantified, thus mainly accounting for the loss in carbon balance.

General characterization. X-ray diffraction analysis was conducted on a PANalytical X-Pert PRO diffractometer, using Cu-Kα radiation at 40 kV and 20 mA. The data were recorded over a 2θ range of 10–80°.

The TEM images were obtained by a JEOL JEM-2100 field emission transmission electron microscope at an accelerating voltage of 200 kV and the calculation of the size distribution of the platinum particles was based on more than 150 particles in the TEM images.

X-ray photoelectron spectra analysis was conducted on ESCALAB250Xi photoelectron spectrometer (Thermo) using Al-Kα (1,486.6 eV) as the exciting source. The basic pressure of the system was 3×10^{-8} Pa; the binding energy was calibrated to the C 1*s* signal (284.6 eV) as a reference.

Photoluminescence experiments were measured on a Photon Technology International QM 400 fluorescence spectrophotometer using a xenon lamp as the excitation source at room temperature; the excitation wavelength was 330 nm.

FT-IR spectra were collected on a Bruker Tensor 27 instrument. The catalyst samples (~30 mg) were pressed into a self-supporting disk (13 mm in diameter). To investigate the adsorption mode of the fatty acids on the catalysts, a trace amount of diluted stearic acid solvent (dissolved in acetonitrile) was added dropwise onto samples after the background spectra were collected. The sample was dried in air and the spectra were then collected. In situ FT-IR studies were also employed to obtain information about CO adsorption on catalysts and the interaction between H_2 and the catalysts. The catalyst sample (~30 mg) was placed in a homemade infrared quartz cell that is attached to a closed glass-circulation system; the quartz cell was then vacuumed, the sample heated to 300 °C for 1 h and subsequently cooled to 30 °C. Background spectra were collected before CO or H_2 injection; highly pure CO or H_2 were supplied from a gas cylinder. For the study of CO adsorption on the catalysts, the spectra were recorded after the system had been vacuumed for 30 min to remove the physically absorbed CO, whereas the spectra were collected at different exposure times for the study of the interaction between H_2 and the catalysts.

EPR spectra were collected on a Bruker spectrometer in the X-band at 77 K with a field modulation of 100 kHz. The microwave frequency was maintained at 9.4 GHz. After catalysts were added into a paramagnetic tube, the inner atmosphere was first replaced by highly pure argon and sequentially purged by highly pure H_2.

TPD experiments were conducted in a U-type quartz tube connected to a mass spectrometer (GSD320 Thermostar); 400 mg of catalyst sample was placed in a U-type quartz tube, heated to 450 °C and kept for 60 min in argon flow (30 ml min^{-1}) to remove adsorbed species from catalyst surface. When the sample was cooled down to 25 °C, the flow was switched to H_2 (30 ml min^{-1}) for 60 min, followed by purging with Ar (30 ml min^{-1}) for 40 min. The sample was then heated to 450 °C with a ramp rate of 10 °C per min^{-1} in argon flow and the TPD profiles were recorded simultaneously.

The AQE measurement was carried out using a Pyrex top-irradiation-type reaction vessel and a xenon lamp (300 W) fitted with a filter of 365 nm. The number of photons reaching the reaction solvent was measured by a calibrated silicon photodiode (LS-100, KEO Instruments) and the AQE was calculated as follows:

$$\text{AQE} = \frac{n(\text{Feedstock converted})}{n(\text{Photons irradiated})} \times 100\% \quad (6)$$

We assumed that one absorbed photon could convert one molecule of feedstock, and the AQE measured was conducted at a low conversion (≤20%). The AQE is 5.6 ± 0.4% (365 nm) for stearic acid conversion over Pt/TiO_2 in H_2 atmosphere (0.1 MPa).

Data availability

The data that support the plots within this paper and other findings of this study are available from the corresponding author on reasonable request.

Received: 11 July 2019; Accepted: 7 January 2020;
Published online: 19 February 2020

References

1. Anthonykutty, J. M. et al. Value added hydrocarbons from distilled tall oil via hydrotreating over a commercial NiMo catalyst. *Ind. Eng. Chem. Res.* **52**, 10114–10125 (2013).
2. Kunkes, E. L. et al. Catalytic conversion of biomass to monofunctional hydrocarbons and targeted liquid-fuel classes. *Science* **322**, 417–421 (2008).
3. Deneyer, A. et al. Direct upstream integration of biogasoline production into current light straight run naphtha petrorefinery processes. *Nat. Energy* **3**, 969–977 (2018).
4. Luo, N. et al. Visible-light-driven coproduction of diesel precursors and hydrogen from lignocellulose-derived methylfurans. *Nat. Energy* **4**, 575–584 (2019).
5. Zhao, C., Brück, T. & Lercher, J. A. Catalytic deoxygenation of microalgae oil to green hydrocarbons. *Green. Chem.* **15**, 1720–1739 (2013).
6. Lestari, S., Maki-Arvela, P., Beltramini, J., Lu, G. Q. & Murzin, D. Y. Transforming triglycerides and fatty acids into biofuels. *ChemSusChem* **2**, 1109–1119 (2009).

7. Abdul Kapor, N. Z., Maniam, G. P., Rahim, M. H. A. & Yusoff, M. M. Palm fatty acid distillate as a potential source for biodiesel production-a review. *J. Clean. Prod.* **143**, 1–9 (2017).
8. Haas, M. J. Improving the economics of biodiesel production through the use of low value lipids as feedstocks: vegetable oil soapstock. *Fuel Process. Technol.* **86**, 1087–1096 (2005).
9. Mäki-Arvela, P. et al. Catalytic deoxygenation of tall oil fatty acid over palladium supported on mesoporous carbon. *Energy Fuels* **25**, 2815–2825 (2011).
10. Gosselink, R. W. et al. Reaction pathways for the deoxygenation of vegetable oils and related model compounds. *ChemSusChem* **6**, 1576–1594 (2013).
11. Zhang, J. & Zhao, C. Development of a bimetallic Pd-Ni/HZSM-5 catalyst for the tandem limonene dehydrogenation and fatty acid deoxygenation to alkanes and arenes for use as biojet fuel. *ACS Catal.* **6**, 4512–4525 (2016).
12. Snåre, M., Kubičková, I., Mäki-Arvela, P., Eränen, K. & Murzin, D. Y. Heterogeneous catalytic deoxygenation of stearic acid for production of biodiesel. *Ind. Eng. Chem. Res.* **45**, 5708–5715 (2006).
13. Zhang, Z. et al. Catalytic decarbonylation of stearic acid to hydrocarbons over activated carbon-supported nickel. *Sustain. Energy Fuels* **2**, 1837–1843 (2018).
14. Peng, B., Yuan, X., Zhao, C. & Lercher, J. A. Stabilizing catalytic pathways via redundancy: selective reduction of microalgae oil to alkanes. *J. Am. Chem. Soc.* **134**, 9400–9405 (2012).
15. Schwarz, J. & König, B. Decarboxylative reactions with and without light—a comparison. *Green. Chem.* **20**, 323–361 (2018).
16. Kraeutler, B. & Bard, A. J. Heterogeneous photocatalytic decomposition of saturated carboxylic acids on titanium dioxide powder. Decarboxylative route to alkanes. *J. Am. Chem. Soc.* **100**, 5985–5992 (1978).
17. Heciak, A., Morawski, A. W., Grzmil, B. & Mozia, S. Cu-modified TiO_2 photocatalysts for decomposition of acetic acid with simultaneous formation of C1–C3 hydrocarbons and hydrogen. *Appl. Catal. B* **140-141**, 108–114 (2013).
18. Betts, L. M., Dappozze, F. & Guillard, C. Understanding the photocatalytic degradation by P25 TiO_2 of acetic acid and propionic aicd in the pursuit of alkane production. *Appl. Catal. A* **554**, 35–43 (2018).
19. Ngo, S. et al. Kinetics and mechanism of the photocatalytic degradation of acetic acid in absence or presence of O_2. *J. Photochem. Photobiol. A* **339**, 80–88 (2017).
20. Holzhäuser, F. J. et al. Electrochemical cross-coupling of biogenic di-acids for sustainable fuel production. *Green. Chem.* **21**, 2334–2344 (2019).
21. Manley, D. W. et al. Unconventional titania photocatalysis: direct deployment of carboxylic acids in alkylations and annulations. *J. Am. Chem. Soc.* **134**, 13580–13583 (2012).
22. Manley, D. W. & Walton, J. C. A clean and selective radical homocoupling employing carboxylic acids with titania photoredox catalysis. *Org. Lett.* **16**, 5394–5397 (2014).
23. dos Santos, T. R., Harnisch, F., Nilges, P. & Schroder, U. Electrochemistry for biofuel generation: transformation of fatty acids and triglycerides to diesel-like olefin/ether mixtures and olefins. *ChemSusChem* **8**, 886–893 (2015).
24. Creusen, G., Holzhäuser, F. J., Artz, J., Palkovits, S. & Palkovits, R. Producing widespread monomers from biomass using economical carbon and ruthenium–titanium dioxide electrocatalysts. *ACS Sustain. Chem. Eng.* **6**, 17108–17113 (2018).
25. van der Klis, F., van den Hoorn, M. H., Blaauw, R., van Haveren, J. & van Es, D. S. Oxidative decarboxylation of unsaturated fatty acids. *Eur. J. Lipid Sci. Technol.* **113**, 562–571 (2011).
26. Cassani, C., Bergonzini, G. & Wallentin, C. J. Photocatalytic decarboxylative reduction of carboxylic acids and its application in asymmetric synthesis. *Org. Lett.* **16**, 4228–4231 (2014).
27. Griffin, J. D., Zeller, M. A. & Nicewicz, D. A. Hydrodecarboxylation of carboxylic and malonic acid derivatives via organic photoredox catalysis: substrate scope and mechanistic insight. *J. Am. Chem. Soc.* **137**, 11340–11348 (2015).
28. Hamid, S. et al. Photocatalytic conversion of acetate into molecular hydrogen and hydrocarbons over Pt/TiO_2: pH dependent formation of kolbe and Hofer–Moest products. *J. Catal.* **349**, 128–135 (2017).
29. Al-Azri, Z. H. N. et al. The roles of metal co-catalysts and reaction media in photocatalytic hydrogen production: performance evaluation of M/TiO_2 photocatalysts (M = Pd, Pt, Au) in different alcohol–water mixtures. *J. Catal.* **329**, 355–367 (2015).
30. Panagiotopoulou, P. & Kondarides, D. I. Effects of promotion of TiO_2 with alkaline earth metals on the chemisorptive properties and water–gas shift activity of supported platinum catalysts. *Appl. Catal. B* **101**, 738–746 (2011).
31. Alexeev, O. S., Chin, S. Y., Engelhard, M. H., Ortiz-Soto, L. & Amiridis, M. D. Effects of reduction temperature and metal–support interactions on the catalytic activity of Pt/γ-Al_2O_3 and Pt/TiO_2 for the oxidation of CO in the presence and absence of H_2. *J. Phys. Chem. B* **109**, 23430–23443 (2005).
32. Parsons, R. The rate of electrolytic hydrogen evolution and the heat of adsorption of hydrogen. *Trans. Faraday Soc.* **34**, 1053–1063 (1958).
33. Heller, A., Aharon-Shalom, E., Bonner, W. A. & Miller, B. Hydrogen-evolving semiconductor photocathods: nature of the junction and function of the platinum group metal catalyst. *J. Am. Chem. Soc.* **104**, 6942–6948 (1982).
34. Wen, B., Li, Y., Chen, C., Ma, W. & Zhao, J. An unexplored O_2-involved pathway for the decarboxylation of saturated carboxylic acids by TiO_2 photocatalysis: an isotopic probe study. *Chem. Eur. J.* **16**, 11859–11866 (2010).
35. Panayotov, D. A. & Yates, J. T. Charge exchange between TiO_2 and a polyfunctional chemisorbed molecule—the involvement of electrophilic groups. *Chem. Phys. Lett.* **399**, 300–306 (2004).
36. Panayotov, D. A. & Yates, J. T. Spectroscopic detection of hydrogen atom spillover from Au nanoparticles supported on TiO_2: use of conduction band electrons. *J. Phys. Chem. C* **111**, 2959–2964 (2007).
37. Li, J. et al. Synergistic effect of surface and bulk single-electron-trapped oxygen vacancy of TiO_2 in the photocatalytic reduction of CO_2. *Appl. Catal. B* **206**, 300–307 (2017).
38. Hurum, D. C., Agrios, A. G., Gray, K. A., Rajh, T. & Thurnauer, M. C. Explaining the enhanced photocatalytic activity of Degussa P25 mixed-phase TiO_2 using EPR. *J. Phys. Chem. B* **107**, 4545–4549 (2003).
39. Prins, R. Hydrogen spillover. Facts and fiction. *Chem. Rev.* **112**, 2714–2738 (2012).
40. Schrauben, J. N. et al. Titanium and zinc oxide nanoparticles are proton-coupled electron transfer agents. *Science* **336**, 1298–1301 (2012).
41. Karim, W. et al. Catalyst support effects on hydrogen spillover. *Nature* **541**, 68–71 (2017).
42. Porosoff, M. D. & Chen, J. G. Trends in the catalytic reduction of CO_2 by hydrogen over supported monometallic and bimetallic catalysts. *J. Catal.* **301**, 30–37 (2013).
43. Chen, H.-Y. T., Tosoni, S. & Pacchioni, G. Hydrogen adsorption, dissociation, and spillover on Ru_{10} clusters supported on anatase TiO_2 and tetragonal ZrO_2 (101) surfaces. *ACS Catal.* **5**, 5486–5495 (2015).
44. Wang, X., Wu, G., Guan, N. & Li, L. Supported Pd catalysts for solvent-free benzyl alcohol selective oxidation: effects of calcination pretreatments and reconstruction of Pd sites. *Appl. Catal. B* **115-116**, 7–15 (2012).
45. Panagiotopoulou, P. & Kondarides, D. I. Effects of alkali promotion of TiO_2 on the chemisorptive properties and water–gas shift activity of supported noble metal catalysts. *J. Catal.* **267**, 57–66 (2009).
46. Weng, Z., Ni, X., Yang, D., Wang, J. & Chen, W. Novel photopolymerizations initiated by alkyl radicals generated from photocatalyzed decarboxylation of carboxylic acids over oxide semiconductor nanoparticles: extended photo-Kolbe reactions. *J. Photochem. Photobiol., A* **201**, 151–156 (2009).
47. Liang, H. et al. Porous TiO_2/Pt/TiO_2 sandwich catalyst for highly selective semihydrogenation of alkyne to olefin. *ACS Catal.* **7**, 6567–6572 (2017).
48. Pattanaik, B. P. & Misra, R. D. Effect of reaction pathway and operating parameters on the deoxygenation of vegetable oils to produce diesel range hydrocarbon fuels: a review. *Renew. Sustain. Energy Rev.* **73**, 545–557 (2017).
49. Hill, J., Nelson, E., Tilman, D., Polasky, S. & Tiffany, D. Environmental, economic, and energetic costs and benefits of biodiesel and ethanol biofuels. *Proc. Natl Acad. Sci. USA* **103**, 11206–11210 (2006).
50. Wang, Y. et al. Heterogeneous ceria catalyst with water-tolerant Lewis acidic sites for one-pot synthesis of 1,3-diols via prins condensation and hydrolysis reactions. *J. Am. Chem. Soc.* **135**, 1506–1515 (2013).
51. Li, R., Han, H., Zhang, F., Wang, D. & Li, C. Highly efficient photocatalysts constructed by rational assembly of dual-cocatalysts separately on different facets of $BiVO_4$. *Energy Environ. Sci.* **7**, 1369–1376 (2014).
52. Zhang, Y., Zhang, N., Tang, Z.-R. & Xu, Y.-J. Identification of Bi_2WO_6 as a highly selective visible-light photocatalyst toward oxidation of glycerol to dihydroxyacetone in water. *Chem. Sci.* **4**, 1820–1824 (2013).
53. Henderson, M., White, J. M., Uetsuka, H. & Onishi, H. Selectivity changes during organic photooxidation on TiO_2: role of O_2 pressure and organic coverage. *J. Catal.* **238**, 153–164 (2006).
54. Jenišťová, K. et al. Hydrodeoxygenation of stearic acid and tall oil fatty acids over Ni-alumina catalysts: influence of reaction parameters and kinetic modelling. *Chem. Eng. J.* **316**, 401–409 (2017).

Acknowledgements

This work was supported by the Strategic Priority Research Program of the Chinese Academy of Sciences (grant no. XDB17000000) and the National Natural Science Foundation of China (grant nos. 21721004, 21690082, 21690084, 21690080, 21711530020).

Author contributions

Z.H. designed and conducted most of the experiments, and wrote the manuscript. Z.Z. carried out the life-cycle assessment and wrote the manuscript. C.Z. contributed to experiment design and manuscript revisions. J.L. performed the DFT study. H.L., N.L. and J.Z. contributed to product analysis, photoreactor design and mechanism investigation. General guidance, project directing and manuscript revisions were done by F.W.

Competing interests

The authors declare no competing interests.

Additional information

Supplementary information is available for this paper at https://doi.org/10.1038/s41929-020-0423-3.

Correspondence and requests for materials should be addressed to F.W.